JBC Papers in Press. Published on May 30, 2017 as Manuscript M117.789164
The latest version is at http://www.jbc.org/cgi/doi/10.1074/jbc.M117.789164

The UbiK protein is an accessory factor necessary for bacterial ubiquinone (UQ) biosynthesis and forms a complex with the UQ biogenesis factor UbiJ

Laurent Loiseau[1], Cameron Fyfe[2], Laurent Aussel[1], Mahmoud Hajj Chehade[3,4], Sara B. Hernández[5], Bruno Faivre[2], Djemel Hamdane[2], Caroline Mellot-Draznieks[2], Bérengère Rascalou[3,4], Ludovic Pelosi[3,4], Christophe Velours[6], David Cornu[7], Murielle Lombard[2], Josep Casadesús[5], Fabien Pierrel*[3,4], Marc Fontecave*[2] and Frédéric Barras*[1]

[1]Aix Marseille Université, CNRS, LCB UMR 7283, IMM, 13402, Marseille, France. [2] Laboratoire de Chimie des Processus Biologiques, UMR8229 CNRS, Collège de France, Université Pierre et Marie Curie, 11 place Marcelin Berthelot, 75 231 Paris Cedex 05, France. [3]Univ. Grenoble Alpes, Laboratoire Technologies de l'Ingénierie Médicale et de la Complexité - Informatique, Mathématiques et Applications, TIMC-IMAG, UMR 5525, 38000 Grenoble, France. [4]CNRS, TIMC-IMAG, 38000 Grenoble, France. [5]Departamento de Genética, Universidad de Sevilla, Sevilla, Spain. [6]Institut de Biologie Integrative de la cellule, Plateforme Interactions des Macromolécules, I2BC, UMR 9198 CNRS, Bât 430F, 91405 Orsay Cedex, France. [7]Institut de Biologie Integrative de la cellule, Plateforme SICaPS, I2BC, CNRS, Centre de Recherche de Gif, SICaPS, F-91198 Gif-sur-Yvette Cedex, France.

Running title: *UbiK and ubiquinone biosynthesis*

To whom correspondence should be addressed:
Frédéric Barras, LCB-CNRS, 31 chemin Joseph Aiguier, 13009 Marseille, France. Email: barras@imm.cnrs.fr. **Marc Fontecave**, Laboratoire de Chimie des Processus Biologiques, Collège de France, 11 place Marcelin Berthelot, 75231 Paris Cedex 05, France. Email: mfontecave@cea.fr. **Fabien Pierrel**, Laboratoire TIMC-IMAG, Domaine de la Merci, 38700 La Tronche, France. Email: fabien.pierrel@univ-grenoble-alpes.fr.

Keywords: Coenzyme Q, ubiquinone, electron transfer, respiratory chain, *Escherichia coli*.

ABSTRACT

Ubiquinone (UQ), also referred to as coenzyme Q, is a widespread lipophilic molecule in both prokaryotes and eukaryotes in which it primarily acts as an electron carrier. Eleven proteins are known to participate in UQ biosynthesis in *Escherichia coli*, and we recently demonstrated that UQ biosynthesis requires additional, nonenzymatic factors, some of which are still unknown. Here, we report on the identification of a bacterial gene, *yqiC*, which is required for efficient UQ biosynthesis, and which we have renamed *ubiK*. Using several methods, we demonstrated that the UbiK protein forms a complex with the C-terminal part of UbiJ, another UQ biogenesis factor we previously identified. We found that both proteins are likely to contribute to global UQ biosynthesis rather than to a specific biosynthetic step, since both ubiK and ubiJ mutants accumulated octaprenylphenol, an early intermediate of the UQ biosynthetic pathway. Interestingly, we found that both proteins are dispensable for UQ biosynthesis under anaerobiosis, even though they were expressed in the absence of oxygen. We also provide evidence that the UbiK-UbiJ complex interacts with palmitoleic acid, a major lipid in *E. coli*. Last, in *Salmonella enterica*, ubiK was required for proliferation in macrophages and virulence in mice. We conclude that although the role of the UbiK-UbiJ complex remains unknown, our results support the hypothesis that UbiK is an accessory factor of Ubi enzymes and facilitates UQ biosynthesis by acting as an assembly factor, a targeting factor, or both.

Isoprenoid quinones are conserved in almost all living organisms and function primarily as electron and proton transporters in photosynthetic and respiratory chains (1). Quinones are composed of a polar redox-active head group coupled to a lipid side chain, which varies in both length and degree of saturation (1). Menaquinone (MK) and ubiquinone (UQ) are the main isoprenoid quinones and differ with respect to the structure of the head group,

a naphthalene ring (in MK) and a benzene ring (in UQ). MK is present in both bacteria and archaea, whereas UQ is restricted to α-, β-, γ-proteobacteria but is also found in eukaryotes (1–3). It is now commonly accepted that MK arose before UQ (4, 5). MK and demethylmenaquinone (DMK) function predominantly in anaerobic respiratory chains whereas UQ is the major electron carrier used for reduction of oxygen by cytochrome oxidases (1). Quinone biosynthesis has been extensively studied in *Escherichia coli* but is still incompletely characterized. The octaprenyl side chain is common to UQ and (D)MK, and chorismate is the precursor of the benzoquinone and napthoquinone rings.

The enzymes catalyzing the different steps of UQ biosynthesis have been described (6). They catalyse the functionalization (prenylation, decarboxylation, hydroxylation and methylation) of the phenyl ring of the 4-hydroxybenzoate precursor. In total 11 proteins, named from UbiA-to-J and UbiX are required for UQ biosynthesis. The hydroxylases UbiI, UbiF and UbiH use dioxygen as a co-substrate and are therefore active only in aerobic conditions (7, 8). The hydroxylases that participate to anaerobic UQ biosynthesis have yet to be identified (6). It is noticeable that only UbiE, a methylase, participates to both UQ and MK biosynthesis. Our recent investigations demonstrated that UQ biosynthesis requires additional factors that seem not to carry out enzymatic function. For example, we have recently discovered that UbiJ is required for UQ biosynthesis in aerobic conditions in both *E. coli* and *Salmonella enterica* (9). The role of UbiJ in UQ biosynthesis remains however enigmatic.

In the present study, we discovered a novel gene, namely *yqiC*, important for UQ biosynthesis under aerobiosis in *E. coli* and *S. enterica*. Contrary to a recent report (10), MK biosynthesis was not impaired in *yqiC* mutant. We therefore propose to change the name of *yqiC* into *ubiK*. The protein from *E. coli* was characterized biochemically and structurally. Interestingly, we demonstrate that UbiK physically interacts with UbiJ and forms an $UbiK_2$-$UbiJ_1$ complex. A *Salmonella ubiK* mutant is growth-deficient under aerobic conditions and the defect is exacerbated at higher temperatures. Consistently, *Salmonella ubiK* mutant is defective for proliferation in macrophages and mice infection. Overall, our results demonstrate the implication of UbiK in aerobic UQ biosynthesis and provide an additional illustration of the importance of UQ for pathogenic bacteria proliferation.

RESULTS

ubiK *is a new gene involved in aerobic UQ_8 biosynthesis*-A high-throughput study previously analyzed the growth of *E. coli* strains from the Keio single gene deletion library in more than 300 conditions and established a phenotypic signature for each mutant strain (11). Functional connection between genes with correlated phenotypic signatures could be predicted (11) and the phenomic profiles of most *ubi* mutants were indeed highly correlated (http://ecoliwiki.net/tools/chemgen/).

Interestingly, the *ubiI* mutant had the highest correlation coefficient with the *yqiC* mutant (hereafter called *ubiK*), prompting us to investigate whether *ubiK* might play a role in UQ_8 biosynthesis.

The *ubiK* mutant had no growth defect in LB medium under aerobic conditions (figure S1A). Its UQ_8 content, as determined by HPLC analysis coupled to electrochemical detection (ECD), decreased down to 18% compared to the wild-type strain (Fig. 1A and 1B). Complementation of the *ubiK* mutant with a plasmid carrying *ubiK* restored the wild-type UQ_8 level (Fig. 1A and 1B). DMK_8 and MK_8 were optimally detected at 247 nm (Fig. S1B) and we found that the levels of DMK_8 were unchanged in the *ubiK* mutant (Fig. 1C), while those of MK_8 increased slightly (Fig. 1D). HPLC chromatograms recorded at 275 nm showed a compound that eluted at 6.4 min, right after UQ_8 in the *ubiK* mutant (Fig. S1C). Mass spectrometry analysis revealed a main peak at *m/z* 656.5 ($M+NH_4^+$) consistent with octaprenylphenol (OPP, $C_{46}H_{70}O$) (Fig. S1D). The accumulation of OPP, an intermediate in the biosynthesis of UQ_8, has been observed previously in several *ubi* mutants deficient in UQ_8 (12, 13). The increased level of OPP in the Δ*ubiK* mutant was diminished to the WT level upon transformation by the plasmid carrying *ubiK* (Fig. 1E), showing that OPP accumulation correlated with UQ_8 deficiency. The UQ_8 content of the *ubiK* mutant strain after anaerobic growth in LB was found similar to WT (Fig. 1F). Finally, via insertion of a sequential affinity purification tag (SPA-tag) at the 3' end of the *ubiK* gene in the *E. coli* chromosome, UbiK levels were quantified by Western blot

analysis after growth under aerobic and anaerobic conditions. We also analyzed the levels of SPA-tagged UbiE and UbiJ. Levels of the three proteins were not influenced by the growth conditions (Fig. 1G). This result was consistent with a recent study, which demonstrated that *ubiJ* and *ubiK* genes were regulated neither by Fnr nor by ArcA, two major transcription factors that respond to oxygen levels (14). Altogether, our results showed that deletion of the *ubiK* gene impacts UQ_8 biosynthesis in aerobic conditions but does not decrease (D)MK biosynthesis.

UbiK is almost exclusively present in Proteobacteria-E.coli UbiK (UniProtKB entry Q46868) is a 96-residue protein which belongs to the BMFP (*Brucella* Membrane Fusogenic Protein) superfamily (Pfam PF04380). Bioinformatics analysis revealed that the 596 members of the BMFP family known to date (Pfam 30.0, March 2017, http://xfam.org/) are almost exclusively found in α-, β- and γ-proteobacteria, where UQ_8 is present (Fig. S2). Interestingly, *ubiK* sequences are not found in the archaebacterial kingdom where MK is the major quinone (1). This exclusive presence of *ubiK* in the proteobacteria phylum is consistent with the involvement of *ubiK* in UQ_8 biosynthesis and not in MK biosynthesis. An alignment of a subset of UbiK sequences from diverse proteobacteria species is shown in Fig. S3. The average sequence identity of all proteins from this family is 34%. One should note that the C-terminal end of UbiK sequences, corresponding to the last 16 amino acid residues in the *E. coli* protein, is poorly conserved among all different species. Consistent with this, we found the deletion of the C-terminus (residues 81-96) to have no effect on UbiK function since this construct yielded wild-type levels of UQ_8 in the Δ*ubiK* strain (not shown).

UbiK forms a trimer-The *ubiK* gene from *E.coli* was cloned without any tag into a pACYCDuet-1 plasmid and the protein was over-expressed in BL21 (DE3) *E.coli* strain. High yield of pure and soluble UbiK could be obtained (10 mg/L culture). In order to determine its absolute molar mass, multi-angle light scattering coupled to size exclusion chromatography (SEC-MALS) experiments were performed. UbiK showed a single homogeneous peak with a molecular mass of 32 kDa (Rh = 2.9 ± 0.08 nm), thus corresponding to a trimer (M_w for monomer = 11.3 kDa), with an elongated hydrodynamic shape (f/f0 = 1.5) (Fig. 2A). Its secondary structure was analyzed by circular dichroism (CD) spectroscopy. The CD spectrum of UbiK exhibited two minima at 208 and 222 nm, indicating the prevalence of helices (Fig. 2B). Analysis of the spectrum using K2D3 and CDSSTR software allowed to estimate percentage for helical structure of 52-55 %, for random coils of 42-45 %, and for β-sheets of 3-4 %. Using analytical ultracentrifugation with fluorescence detection, a trimeric oligomer was observed at a concentration down to 250 nM, at which point the protein aggregates suggesting it is unstable as a monomer. A thermal unfolding experiment was performed by monitoring the CD spectrum of UbiK as a function of temperature (Fig. S4). The midpoint of the unfolding transition (T_M) was 66.5 ±0.1°C and the observed conformational transitions were fully reversible which allowed us to determine the Van't Hoff enthalpy of unfolding, ΔH = 250.6 +/- 2 kJ/mol. These values are indicative of a very stable protein, in accordance with a coiled-coil protein structure (15).

Structural model of UbiK-UbiK and human Brick1 share 25% sequence identity. Human Brick1 (UniProtKB entry Q8WUW1) forms the core subunit of the Wave (Wiskott-Aldrich VErprolin proteins) complex involved in actin polymerization. Brick1 contributes to the architecture of the complex by serving as a platform on which the four other proteins assemble. In order to gain insights into the structural organization of the UbiK trimer, a structural model was generated using Swiss-Model (http://swissmodel.expasy.org/). The PDB codes for the main templates used were: 3PP5 (Brick1 from *Dictyostelium discoides*), 3P8C chain E (Brick1 from *Homo sapiens*), and 4LL7 (She3p from *Saccharomyces cerevisiæ*) (16). When purified alone, Brick 1 assembles as an α-helical triple-coiled-coil along a well-conserved hydrophobic patch (17) (Fig. 3A). The hydrophobic core of the Brick1 trimer bundle, is also seen within the UbiK sequence (Fig. S3). The best model of UbiK monomer calculated with Swiss-Model thus consisted of two long aligned α helices connected by a loop in the central core of the protein and disordered domains at the N and C-terminal ends (Fig. 3B). The secondary structures contents of this model matched the ones determined by circular

dichroism (Fig. 2B): approximately 53% of α-helices and 47% of random coils. On this basis we propose a model for the UbiK homotrimer, displaying the same fold as the triple coiled-coil structure in Brick1 (Fig. 3C).

UbiK interacts with other Ubi proteins- To answer whether UbiK interacts with other Ubi proteins *in vivo*, we used the bacterial BACTH two-hybrid reporter system that monitors both direct and indirect interactions. This method is based on functional complementation between adenylate cyclase fragments T18 and T25 expressed from two compatible plasmids (18). Adenylate cyclase activity is restored only when proteins fused to T18 and T25 interact. In line with our results about the oligomerization of UbiK, it was found to interact with itself (Fig. 4A and 4B). In addition, UbiK interacted with the following Ubi proteins: UbiB, E, F, G, H, I, J, and X (Fig. 4A and 4B). More specifically, UbiK interacted with UbiE, F, G, H, I, J, K and X proteins regardless of if it was fused to the T18 or T25 proteins. UbiK also interacted with UbiB but only when it is fused to the T18 moiety. Last, UbiK failed to interact with UbiA, UbiC and UbiD (Fig. 4A and 4B). Altogether, these results suggested that UbiK plays a pivotal role in *E. coli* UQ_8 biosynthesis.

UbiK interacts directly with UbiJ-To further substantiate the idea that UbiK had a pleiotropic role in UQ_8 biosynthesis, we used co-expression and co-purification assays to test the connection between UbiK and other Ubi proteins. For this we choose a subset of Ubi candidates among those suggested to partner with UbiK by the bacterial two-hybrid assay above. Likewise, Ubi G, J, X, E and J were fused to a His_6-tag and UbiK to an S-tag. Soluble fractions containing the His_6-tagged proteins were purified on Ni-NTA resin, and UbiK was detected exclusively in extracts containing UbiJ-His_6 (Fig. 5A). Interactions between the UbiK and UbiJ proteins were further investigated using pull-down assays. *ubiK*, *ubiJ* and *sufC* (used as a negative control) genes were fused at their 5′-end with the *malE* gene. The chimeric proteins, MBP-UbiK and MBP-SufC were purified in strains carrying a chromosomal copy of the *his$_6$-ubiJ* gene while on the other hand MBP-UbiJ and MBP-SufC were purified from a strain containing an *ubiK-SPA* gene. Soluble extracts of each strain were loaded on an amylose column. The column was then extensively washed and finally a solution of maltose (10 mM) was applied. MBP-UbiK and His_6-UbiJ were co-eluted (Fig. 5B, lane 2) as MBP-UbiJ and UbiK-SPA (Fig. 5B, lane 4). MBP-SufC was always eluted alone (Fig. 5B, lanes 1 and 3). His_6-UbiJ and UbiK-SPA were identified by immunoblotting using anti-His (Gene Tex) and anti-Flag (Sigma) antibodies, respectively. Thus, biochemical analyses allowed us to confirm that UbiK interacts with UbiJ. Last, yeast two-hybrid based tests were run as they report on direct interactions and might eventually allow to pinpoint zones of interaction. Evidence of an UbiK-UbiJ direct interaction was found to depend on the C-terminus 50 amino-acids of UbiJ only (UbiJ 151-201) (Fig. 5C). No interaction was observed using the N-terminus part of UbiJ (Data not shown). Altogether, these results established unambiguously that UbiK and UbiJ interact specifically and form a complex *in vivo*.

Biochemical characterization of the E. coli UbiK-UbiJ complex-E. coli UbiK and UbiJ were co-expressed in *E.coli* BL21 strain, using the T7 promoter pETDuet-1 expression vector. A two-step purification consisting of an affinity column (His Trap HP) followed by size exclusion chromatography (HiLoad 16/600 Superdex 200 pg) resulted in three well-separated protein peaks (Fig. S5). The low-molecular mass peak, called P3, with a molar mass of approximately 18-20 kDa based on SDS-PAGE, was analyzed by ESI-MS and peptide mass fingerprint (Fig. S6). P3 did not contain any UbiK protein but only two main fragments of UbiJ: one major species lacking the last 56 C-terminal residues (UbiJ Δ146-201) and one minor species, lacking the last 63 C-terminal residues (UbiJ Δ138-201) (Fig. S5 and S6). These truncated forms are most likely a result of proteolysis during purification. In contrast, the first (minor, P1) and the second (major, P2) peaks contained both UbiK and UbiJ in seemingly different ratios. They were both subjected to SEC-MALS and analytical ultracentrifugation. SEC-MALS analysis of P2, eluting at 13.4 ml, led to a single molar mass (49 kDa) with a hydrodynamic radius of 3.6 ± 0.4 nm and a frictional ratio f/f0 of 1.7 that matches an elongated hetero-complex of two monomers of UbiK (28 kDa) and one monomer of UbiJ (21 kDa) (Fig. 6A). Sedimentation velocity experiments revealed three different species,

with the sedimentation coefficients: 2.8 $S_{20,W}$ (~60%), corresponding to a 2:1 UbiK-UbiJ complex; 3.8 $S_{20,W}$ (~20%); 5.6 $S_{20,W}$ (~10%) corresponding to larger oligomeric species (Fig. S7A). The stoichiometry of the dominant species remained unchanged with increased protein concentration (Fig. S7B), indicating a stable UbiK-UbiJ (2:1) hetero-complex. P1 eluting at 12.8 ml (Fig. 6B) consists mainly of two species: the minor component is UbiK homo-trimer and the major component is a hetero-trimer of UbiK-UbiJ (2:1). Evidence for the presence of the UbiK homo-trimer in P1 is given by sedimentation velocity experiments. The 2.2 $S_{20,W}$ species in P1 is only seen by interference (Fig. S7C), and not in absorbance (Fig. S7D), thus indicating the presence of UbiK only, and has furthermore a sedimentation coefficient similar to that of the homo-trimeric UbiK (2.1 $S_{20,W}$) (Fig. S7E). The hetero-trimer of UbiK-UbiJ in P1 has a different sedimentation coefficient (3.2 $S_{20,W}$) than the main species in P2 (2.8 $S_{20,W}$) probably due to having a different 3D conformation. This is further suggested by the varying frictional ratio seen between P2 and P1, 1.80 f/f0 and 1.55 f/f0 respectively. This higher frictional ratio seen for P2 highlights its more elongated form and explains the higher sedimentation coefficient.

To further confirm the UbiJ C-terminal interaction with UbiK, we produced three plasmids encoding UbiK without an Stag alongside three truncated versions of UbiJ (His tag), UbiJ Δ121-201, UbiJ Δ1-120 and UbiJ Δ1-145 (Fig. S8). Upon coexpression and purification of UbiK and UbiJ truncations by nickel affinity column, we observed that the C-terminus of UbiJ (UbiJ Δ1-120 and UbiJ Δ1-145) is essential for binding UbiK and that the N-terminus (UbiJ Δ121-201) is not able to bind UbiK. These *in vitro* results confirm the *in vivo* double hybrid assays (Fig. 5C) that show that only the C-terminus is responsible for UbiK binding.

In the absence of a three-dimensional structure, we also built a model for the hetero-trimer UbiK-UbiJ complex. Sequence homologies between UbiK and Brick1 and between UbiJ and Sterol Carrier Protein (SCP-2) proteins (Fig. S9 and 6C), which are intracellular lipid transfer proteins, as well as in silico structural predictions allowed us to propose the model shown in Fig. 6D. In this model the UbiK-UbiJ 2:1 heterocomplex results from the formation of a three-helix bundle between two monomers of UbiK and the α-helical C-terminus of one monomer of UbiJ, in full agreement with the latter being responsible for UbiJ binding to UbiK.

UbiK-UbiJ bind lipids-E. coli UbiJ is made of an N-terminal Sterol Carrier Protein (SCP-2) domain (1-120) and a putative C-terminal coiled-coil domain (121-201) (Fig. S9). SCP-2, also known as nonspecific lipid transfer protein, is a small ubiquitous protein of unknown function. Several existing X-ray or NMR structures of SCP-2 proteins revealed the protein accommodates an internal and hydrophobic cavity suitable for lipid binding (19–23). As a matter of fact, fatty acid molecules, such as palmitic and stearic acids, were observed in the various SCP-2 members. Therefore, we tested if a lipid molecule might be bound to purified UbiK-UbiJ complex. The purified UbiK-UbiJ P2 complex was treated with methanol, heated at 95°C and centrifuged. The supernatant was then injected onto an ESI/MS apparatus equipped with a triple TOF detector in a negative mode (Fig. 7). Interestingly, in this supernatant a mass at m/z = 253.22 was identified as palmitoleic acid (commercial standard m/z = 253.23). Palmitoleic acid, (9*Z*)-hexadec-9-enoic acid, is a C_{16} mono-unsaturated lipid which is largely found in *E. coli*, along with other C_{14} and C_{18} fatty acids: it represents 35% of the lipids within the membrane of the bacterium, while palmitic acid represents 45%, vaccenic acid 18% and myristic acid 2%. Similar experiments using UbiK alone revealed no lipid binding (data not shown).

The Salmonella ubiK *gene is required for UQ_8 biosynthesis, intracellular proliferation and virulence in mice*-Previously, we found that *ubiJ* was required for UQ_8 biosynthesis and intracellular proliferation in *Salmonella enterica* (9). Given the functional interaction between UbiK and UbiJ in *E. coli* reported above, we constructed an *ubiK* mutant in *S. enterica* and measured its UQ_8 content. Compared to the wild-type strain, we found a 16-fold decrease in UQ_8 when the *ubiK* mutant was grown in LB under aerobic conditions (Fig. 8A). Complementation of this mutant led to an increase of the UQ_8 level to ~70% of the WT (Fig. S10A). The levels of DMK_8 and MK_8 were not significantly different between Δ*ubiK* and WT strains (Fig. S10B). As already observed in

E. coli, the UQ_8 content of the *ubiK* mutant was not different from that of the WT after growth in anaerobic conditions (Fig. 8A). Next, RAW 264.7 mouse macrophages were infected with the wild-type strain and the *ubiK* mutant. Bacterial proliferation was assayed by calculating the proliferation index as the ratio of the number of intracellular bacteria at 16 h post-infection to that at 2 h post-infection. Because important differences were found in UQ_8 content in function of the presence or the absence of oxygen, bacterial inoculum were grown either aerobically or anaerobically. The *ubiK* mutant exhibited proliferation index 16-fold lower compared to its wild-type parent with an aerobic inoculum and 3-fold lower with an anaerobic inoculum (Fig. 8B). Interestingly, the intracellular proliferation of the *ubiK* mutant was found to be higher when the infection was performed with an anaerobic inoculum (11) compared with an aerobic inoculum (2.5) (Fig. 8B). Because an *ubiK* mutant was previously shown to exhibit a thermosensitive phenotype in *Salmonella* (24), we monitored the growth of a wild-type and an *ubiK* mutant at different temperatures and found indeed that the growth impairment was exacerbated at higher temperatures (Fig. S10C). Thus, to investigate the impact of the temperature on the intracellular proliferation capacity of the *ubiK* mutant, infection of RAW 264.7 mouse macrophages was carried out at 30°C and 37°C. The proliferation index of the *ubiK* mutant was severely affected compared to the wild-type strain at 37°C (12-fold) whereas the difference was much more reduced at 30°C (2-fold) (Fig. 8C). The UQ_8 deficiency of the *ubiK* mutant compared to the wild-type strain was less severe at 30°C than at 37°C (9-fold and 16-fold, respectively) (Fig. S10D and 8A), which suggest that the increased proliferation index of the *ubiK* mutant at 30°C may be due to the higher UQ_8 content. Lastly, mixed infections of mice were carried out using the *ubiK* mutant and the wild-type strain in order to determine the competitive index (CI) and to compare the virulence of the two strains (25). Mice were infected intraperitoneally and the *ubiK* mutant was found to be highly affected for its virulence in the animal (CI = 0.0005) (Fig. 8D). Collectively, these results confer to *ubiK* a key role in UQ_8 biosynthesis and in *Salmonella* virulence.

DISCUSSION

UQ_8 acts as a membrane-embedded electron shuttle and is a key molecule for bacteria to use respiratory metabolism for growth. Biosynthesis of UQ_8 includes a series of enzymatic steps in which a benzene ring undergoes a series of modifications (prenylation, decarboxylation, methylation, hydroxylation). Recently, however, we obtained evidences that non-enzymatic biogenesis factors might also be required. Indeed, we identified UbiJ as a new factor involved in UQ_8 biosynthesis in *E. coli* and *Salmonella* under aerobiosis (9). In the present study, we identified an additional new biogenesis factor, called UbiK, that is also required for UQ_8 biosynthesis and which is unlikely to carry out any enzymatic function. Phenotypic and biochemical characterization revealed that UbiK and UbiJ function as a complex that contributes to as yet unclear step(s) in UQ_8 biosynthesis. We collected evidences that allow us to discuss their possible role in helping other enzymatic Ubi proteins to carry out their function.

Our results and interpretation differ from a recent study that concluded that UbiK was involved in MK biosynthesis in *Salmonella* (10). This conclusion was based on an analysis of the quinone content of an *ubiK* mutant. We did not confirm such results as, in our analysis, the levels of (D)MK_8 were not decreased in the *ubiK* mutant compared to the wild-type strain in both *E. coli* and *S. typhimurium*. We believe that this discrepancy is due to the erroneous identification of *Salmonella* endogenous MK_8 in the HPLC chromatograms by Wang *et al.* (10). Indeed, these authors used commercial vitamin K2 (MK_4) as a standard to identify the retention time of MK_8 in chromatograms of *Salmonella* lipid extracts, whereas MK_4 and MK_8 have entirely different retention time on C18 columns.

The occurrence of an UbiK-UbiJ complex was demonstrated by using multiple molecular, biochemical and physical methods. Besides all evidences for the occurrence of an UbiK-UbiJ complex, we noticed marked changes in the behavior of UbiJ and UbiK depending on whether the proteins were overexpressed individually or together. Indeed, while UbiK alone is a trimer, it is converted to a dimer upon interaction with one UbiJ monomer and while UbiJ is insoluble on its own it is perfectly soluble when interacting with UbiK. In the absence of a three-dimensional

crystal structure, we are able to propose a model for that complex. In this model an UbiJ monomer and UbiK dimer make a heterotrimeric complex allowed by the formation of a three-helix bundle from two monomers of UbiK and the helical C-terminus of UbiJ.

Human Brick1 (UniProtKB entry Q8WUW1) forms the core subunit of the Wave (Wiskott-Aldrich VErprolin proteins) complex involved in actin polymerization. Interestingly, the 400 kDa Wave complex consists of five proteins and Brick1 (HSPC300) contributes to the architecture of this mega complex by serving as a platform to the other proteins (16). On this basis, one can speculate that UbiK, and by extension the UbiK-UbiJ complex, might participate to some sort of platform. Such a role would be consistent with the fact that none of them is predicted to carry out an enzymatic function, and that inactivation of both drastically reduces the level of UQ_8 but lead only to the accumulation of the early intermediate OPP, which is not diagnostic of a defect in a specific biosynthetic step. The hypothesis that all Ubi enzymes are part of, and function as a mega complex has received some support in bacteria and is well established in eucaryotes (26–28). That the UbiK-UbiJ be instrumental in the formation of such a complex is supported by data of the bacterial 2-hybrids analysis. Indeed, UbiK was found to be connected, directly or not, with most Ubi proteins. Hence it is tempting to think of the UbiK-UbiJ complex as a facilitator of the formation (folding, assembly, nucleation) of a Ubi mega complex. Another possibility, which is not exclusive from the one just discussed, is that UbiK-UbiJ helps location or interaction of the Ubi enzymes with the membrane. Indeed, a conundrum is that while UQ_8 biosynthesis must take place within the membrane environment, only one of the Ubi proteins, UbiA, is actually membrane bound. The obvious need of locating the Ubi enzymes or complex to the membrane could be fulfilled by the UbiK-UbiJ complex. This putative function is consistent with our demonstration that UbiK-UbiJ is able to bind lipids.

During the course of the infection, *Salmonella* can be exposed to different stressful conditions and must negotiate anaerobic and aerobic environments (29). In this work, we provided evidence that UbiK is required for full multiplication in macrophages and full virulence in mice. This is in agreement with a previous study by Carrica *et al.* who reported that *ubiK* was important for *Salmonella* virulence in a mouse model (24). However, because the *ubiK* mutant exhibits a thermosensitive phenotype, it is difficult to sort out the global defect from the specific contribution to virulence. Interestingly, we found the *ubiK* mutant proliferation to be partially recovered when the bacterial inoculum was grown anaerobically or when the infection was carried out at 30°C, two conditions during which UQ_8 levels increased in the *ubiK* background. This is both consistent with our previous proposal for a requirement of UQ_8 for an efficient intracellular proliferation and in support of the hypothesis that *Salmonella* intracellular lifestyle relies on aerobic respiration and oxygen availability to survive and proliferate within host cells.

EXPERIMENTAL PROCEDURES

Bacterial strains and growth conditions- *E. coli* strains were grown in Luria-Bertani (LB) medium at 37°C in Erlenmeyer flasks filled to 1/10 of the maximal volume and shaken at 150 rpm (aerobic conditions). For anaerobic growth, Hungate tubes were used and the LB medium was extensively degassed with Argon before the tubes were closed and autoclaved. Cultures were inoculated through the septum of the Hungate tube with a syringe fitted with a sterile needle. Ampicillin (50 µg/ml), kanamycin (25 µg/ml), and chloramphenicol (25 µg/ml) were added when needed. Deletion of various genes and concomitant insertion of an antibiotic resistance cassette was carried out using lambda Red-mediated recombination (30). Mutations were moved to the wild-type *E. coli* strain MG1655 by P1 transductions and to the wild-type *S. enterica* strain 12023 by P22 transductions.

Plasmid constructions-The *ubiK and ubiJ* inserts were obtained by PCR amplification using MG1655 as template and the oligonucleotides 5-*Eco*RI-*ubiK*/3-*Xho*I-*ubiK* and 5-*Eco*RI-*ubiJ*/3-*Xho*I-*ubiJ*, respectively. *UbiK and ubiJ* inserts were *Eco*RI-*Xho*I digested and inserted into *Eco*RI-*Sal*I-digested pTrc99A or pBAD24 plasmids, yielding the pTrc-*ubiK* and pTrc-*ubiJ* plasmids or pA-*ubiK* and pA-*ubiJ* plasmids, respectively.

In order to overproduce MBP-UbiK and MBP-UbiJ, the *ubiK* and *ubiJ* genes were

cloned into the pMal-c2 vector downstream of the Ptac promoter. The *ubiK* and *ubiJ* inserts were obtained by *Eco*RI-*Hind*III digestion of the pTrc-*ubiK* and pTrc-*ubiJ* plasmid and the restricted fragments were inserted into *Eco*RI-*Sal*I-digested pMal-c2, yielding pMal-*ubiK* and pMal-*ubiJ*.

The pEG202 and pJG4-5 vectors were used to express UbiK, UbiJ and $UbiJ_{50aa}$ proteins fused to the DNA binding protein LexA and to the transcriptional activation motif B42, respectively. The inserts were obtained by PCR using MG1655 chromosomal DNA as a template and 5-*Eco*RI-*ubiK*/3-*Xho*I-*ubiK*, 5-*Eco*RI-*ubiJ*/3-*Xho*I-*ubiJ* and 5-*Eco*RI-$ubiJ_{50aa}$ /3-*Xho*I-*ubiJ* primers. The inserts were digested by *Eco*RI-*Xho*I. The restricted *ubi* genes containing inserts were cloned into the *Eco*RI-*Xho*I digested pEG202 and pJG4-5, yielding the pB42 and pLexA plasmid series, respectively.

To construct pETDuet-*ubiK*-S-tag. The coding sequence of the *E. coli ubiK* gene was PCR amplified from an MG1655 strain by using the 5-*Nde*I-*ubiK* and 3-*Xho*I-del-stop-*ubiK* primers, digested using *Nde*I and *Xho*I, and cloned into pETDuet-1, yielding pETDuet-*ubiK*-S-tag.

To construct pETDuet-*ubiK*-no-tag, the *ubiK* gene was PCR amplified by using the 5-*Nde*I-*ubiK* and 3-*Xho*I-*ubiK* primers, digested using *Nde*I and *Xho*I, and cloned into pETDuet-1, yielding pETDuet-*ubiK*-no-tag.

UbiJ insert was obtained by *Eco*RI-*Hind*III digestion of the pTrc99A-6his-*ubiJ* vector. The restricted fragment was inserted into pETDuet-*ubiK*-S-tag *Eco*RI-*Hind*III-digested, yielding pETDuet-6his-*ubiJ*/*ubiK*-S-tag.

To modify pETDuet-6his-*ubiJ*/*ubiK*-S-tag and remove the S-tag, a TGA stop codon was inserted using 5-*ubiK*stop and 3-*ubiK*stop primers. The pETDuet-6his-*ubiJ*/*ubiK* (without S-tag) was used to generate the three pETDuet-*ubiJ* truncated versions: UbiJ Δ121-201, UbiJ Δ1-120 and UbiJ Δ1-145.

All pETDuet plasmids versions were verified by DNA sequencing and then transformed into *E. coli* BL21 (DE3).

Strain construction- The *yqiC*::Kan mutation from the BW25113 strain (Keio library) was transduced into a MG1655 strain by P1 transduction.

To build the His_6-*ubiJ* strain, an insert carrying the *lacZ-aadA7*(Spc^R)-*ptac-*His_6-*ubiJ-lacZ* gene was obtained after *Pvu*II–*Sca*I digestion of the pGEMT-*aadA7*(Spc^R)-*ptac-*His_6-*ubiJ* vector. In the resulting fragment, the *His6-ubiJ* gene is under the control of the Ptac promoter. Replacement of the *lacZ* allele by the *LacZ-aadA7*(Spc^R)-*ptac-*His_6-*ubiJ-LacZ* gene was carried out in the *ubiJ* strain as described by Datsenko and Wanner (30).

The DY330 *ubiC-SPA* strain encompassing the SPA-tag DNA sequence and the kanamycin antibiotic resistance marker cassette (Kan^R) is used as a template in polymerase chain reaction (PCR) amplification. A 5-*ubiK*-SPA gene-specific forward primer, located immediately upstream of the *ubiK* gene stop codon, and a 3-*ubiK*-Kan gene-specific reverse primer, located immediately downstream of the target gene stop codon, are used to amplify the SPA-tag and Kan^R cassette. The purified PCR product is subsequently targeted to integrate at the 3' end (immediately upstream of the native stop codon) of an *ubiK* gene in BW25113 strain in which the λ-Red recombination machinery is expressed. The *ubiK*-SPA-Kan was transduced through P1 phage from BW25113 to MG1655.

Analyses of the quinone content- Quinone extraction and quantification by HPLC-ECD analyses were performed as previously described (31). UQ_{10} was used as a standard and a precolumn guard cell set at +650 mV allowed the quinones to be detected in their oxidized form. Electrochemical detection (ECD) was performed with a Coulochem III (Thermo Fisher) equipped with a 5011A analytical cell (E1, -650 mV; E2, +650 mV) and UV detection at multiple wavelengths was performed with a diode array detector. The peaks for DMK_8 and MK_8 were integrated from the 247 nm chromatograms and that of OPP from the 275 nm chromatograms. Similarly to the UQ_8 signal, the peak areas were corrected for sample loss during the lipid extraction based on the recovery of the UQ_{10} standard and values were expressed per mg of cell wet weight When mass spectrometry (MS) detection was needed, the flow was divided after the diode array detector with an adjustable split valve (Analytical Scientific Instruments) in order to allow simultaneous EC (60% of the flow) and MS (40% of the flow) detections. MS detection was performed in positive mode with electrospray ionization on a MSQ Plus spectrometer (Thermo Fisher). The probe

temperature was 450°C, the cone voltage was 80 V, and MS spectra were recorded between *m/z* 600 and 880 with a scan time of 0.4 s.

Western Blot analysis-E. coli cells were harvested in exponential phase, washed with PBS buffer and heated at 95°C for 10 min in Laemmli buffer. Equal amount of *E. coli* protein extracts were analyzed on a 15% acrylamide SDS-PAGE gel. Immunoblot analyses were performed with polyclonal antibodies raised against LamB (courtesy of A. Meinke, Intercell AG), monoclonal antibodies raised against FLAG epitope (Sigma-Aldrich) included in the SPA tag (32) and monoclonal antibodies raised against His epitope (Gene Tex). Immunodetection was performed using goat anti-mouse HRP-conjugated (Bethyl Laboratories) or goat anti-rabbit HRP-conjugated (Covalab) and the Clarity Western ECL substrate (Bio-Rad). Primary antibodies were used at the following dilutions: anti-LamB, 1/2000 and anti-FLAG epitope, 1/5000.

Bacterial two-hybrid reporter system-Bacterial two-hybrid reporter system is based on functional complementation between *Bordetella pertussis* adenylate cyclase fragments, T18 and T25, expressed separately from two compatible plasmid replicons (18). Adenylate cyclase activity is restored only when proteins fused to T18 and T25 interact. Functional reconstitution of *B. pertussis* adenylate cyclase in an *E. coli* Δ*cya lac*$^+$ strain is monitored by assaying the activity of a cAMP-CRP-dependent lac promoter of a chromosomally encoded lac operon. Fusions were constructed with T18 and T25 present at the N-terminal of Ubi proteins.

Yeast two-hybrid system-The yeast two-hybrid system assay was performed as described by Golemis *et al*. (33). The β-galactosidase activity from diploid cells, obtained by mating of strains EGY48 and RF206 carrying the appropriate plasmid, was detected on plates containing X-gal (33) and was quantified from liquid culture. The β-galactosidase activity was expressed as nanomoles of *o*-nitrophenyl-β-d-galactoside hydrolysed per minute per milligram of protein. The diploid cells were also assayed for the expression of the *Leu* reporter gene. Diploid strains were grown in liquid selective CM medium lacking leucine.

Pull down of MBP hybrid proteins-MG1655 *ubiK-SPA* cells transformed with pMal-*sufC* and pMal-*ubiJ* and MG1655 *His$_6$-ubiJ* cells transformed with pMal-*sufC* and pMal-*ubiK* were grown at 37°C in 200 ml of LB medium to an OD_{600} of 1.0. Induction was performed with 0.1 mM IPTG, which was added for 3.5 h at 37°C. The bacterial pellet was resuspended in 8 ml of buffer A (100 mM Tris–HCl pH 7.5, 50 mM NaCl) and disrupted twice by French pressure treatment. The cell lysate was centrifuged at high speed for 15 min at 4°C. Supernatants were added to 300µl of amylose resin (New England Biolabs). The mixture was stored for 3.5h at 4°C. The resin was then washed with 30 resin vols of buffer A. The recombinant proteins, MBP–UbiK, MBP–UbiJ and MBP–SufC, were eluted with buffer A added with 10 mM maltose. For detecting His$_6$-UbiJ, 0.5 ml elution fractions concentrated 10X on microcon (Millipore) were analysed by immunoblotting using anti-His antibodies (Gene Tex) while for detecting UbiK-SPA protein, aliquots of the 0.5 ml fractions were analysed using anti-Flag (Sigma) antibodies.

Expression and purification of UbiK-Overexpression was performed in BL21(DE3) *E.coli* strain transformed with pETDuet-*ubiK*-no-tag. Cells were grown with shaking (200 rpm) at 37°C, in LB medium containing ampicillin (100 µg/ml), until they reached A_{600nm} = 0.5, when overexpression was induced by addition of IPTG (0.4 mM). After induction, cells were grown for 4 hours at 37°C, and then harvested by centrifugation at 5000 x *g* for 10 min. All subsequent operations were carried out at 4°C. Cells were resuspended in 5 volumes of buffer B (50 mM Tris-HCl pH 7.5, 20 mM NaCl, 1 mM Pefabloc) and lyzed by sonication (Branson Digital Sonifier, Amplitude 40% for 10 min). Nucleic acids were precipitated by streptomycin sulfate (2% w/v) and the crude extracts were then submitted to ultracentrifugation at 180,000 x *g* for 90 min (Optima XPN-80, rotor 50.2 Ti, Beckman Coulter). The resulting supernatant was loaded onto a Hiprep 26/10 Desalting column (GE Healthcare). The resulting desalted proteins were loaded onto a Hitrap Q FF (5 ml, GE Healthcare) equilibrated with buffer A. Bound

proteins were eluted with a gradient of NaCl (0-500 mM) in 50 mM Tris-HCl pH 7.5 buffer, and UbiK was eluted at 120 mM NaCl. The most pure UbiK fractions were pooled and loaded onto a HiLoad 26/600 Superdex 200 pg equilibrated with 50 mM Tris-HCl pH7.5, 150 mM NaCl. The elution volume of UbiK was 185 ml. UbiK fractions were pooled, frozen in liquid N_2, then stored at - 80°C.

Expression and purification of UbiK-UbiJ complexes-Overexpression was performed in BL21(DE3) *E.coli* strains transformed with pETDuet-6his-*ubiJ*/*ubiK*-S-tag. Cells were grown with shaking (200 rpm) at 37°C, in LB medium containing ampicillin (100 µg/ml), until they reached A_{600nm} = 0.4, when overexpression was induced by addition of IPTG (0.2 mM). After induction, cells were grown for 4 hours at 37°C, and then harvested by centrifugation at 5000 x *g* for 10 min. All subsequent operations were carried out at 4°C. Cells were resuspended in 5 volumes of buffer B and lyzed by sonication (Branson Digital Sonifier, Amplitude 40% for 10 min). Crude extracts were then submitted to ultracentrifugation at 180,000 x *g* for 90 min (Optima XPN-80, rotor 50.2 Ti, Beckman Coulter). The resulting supernatant was loaded onto a Hitrap Chelating HP (5 ml, GE Healthcare) equilibrated with buffer A. Bound proteins were eluted with a gradient of imidazole (0-500 mM) in buffer 50 mM Tris-HCl pH 7.5, 150 mM NaCl. The most pure UbiK-UbiJ complexes fractions were pooled and loaded onto a HiLoad 26/600 Superdex 200 pg equilibrated with 50 mM Tris-HCl pH7.5, 150 mM NaCl. The fractions corresponding to peak 1 and peak 2 fractions were pooled, frozen in liquid N_2, stored at - 80°C, and then submitted to SEC-MALS analysis.

Circular dichroism-Circular dichroïsm in the far-UV region was performed at 20°C using a spectropolarimeter (Jasco J-810) equipped with a water-cooled Peltier unit. UbiK spectra were recorded in a 0.01 mm path length cell (121.QS, Hellma) from 185 to 260 nm with 11 mg/ml UbiK sample in 50 mM Tris HCl, 150 mM NaCl pH 7.5 buffer. For each sample, an averaged spectrum was produce by merging three consecutive scans; the spectra were corrected using buffer baseline measured under the same condition. Data were recorded in mdeg then converted to delta epsilon (Δε, M−1.cm−1). Estimations of secondary structure were predicted by using CDSSTR, SELCON3, CONTIN methods included in the DICHROWEB server (34), or by using K2D3 method (35).

SEC-MALS analyses-Purified UbiK and copurified UbiK-UbiJ P1 and P2 were analyzed using an HPLC-MALS system (Shimadzu) equipped with three detectors, the light scattering detector (mini DAWN TREOS system, Wyatt Technology), the refractive index detector (Optilab T-rEX, Wyatt Technology) and the UV detector from HPLC (SPD-20A, Shimadzu). 200 µg samples of UbiK, UbiK-UbiJ P1 and P2 were injected in a Superdex 200 10/300 GL Increase column (GE Healthcare Life Sciences) equilibrated in 50 mM Tris-Cl pH 7.5, 150 mM NaCl buffer at a flow rate of 0.5 ml min^{-1}. Molar masses of proteins were calculated using ASTRA 6.1 software (Wyatt Technology) using a refractive index increment (dn/dc) value of 0.183 ml g^{-1}. Molecular weight of UbiK and UbiJ within the UbiK-UbiJ complexes were determined by using the protein-conjugate method. This method is based on the use of the three signals (light scattering, absorbance and differential refractive index) to determine the molecular weight of the protein and of the conjugate (DNA, RNA, glycosylation, detergent…) in complex. Formalism of protein-conjugate method was described in Veesler et al., 2009 with protein-detergent complex (36). By analogy, the system can be applied to protein A/protein B complex if mass extinction coefficient are different (ε_A is 2 or 3 times higher than ε_B). As dn/dc of protein is relatively constant (37), dn/dc were fixed to 0.183 ml g^{-1}. α is the weight proportion of protein A, 1-α corresponds to the weight proportion of protein B. C_A and C_B are the respective weight concentrations of protein A and protein B.

$$C_{AB} = \alpha\, C_A + (1-\alpha)\, C_B \qquad (1)$$

$$\left(\frac{dn}{dc}\right)_{AB} = \alpha \left(\frac{dn}{dc}\right)_A + (1-\alpha)\left(\frac{dn}{dc}\right)_B \qquad (2)$$

Using equation (3), the concentration of C_{AB} can be expressed as:

$$C_{AB} = \frac{\Delta n}{\left(\frac{dn}{dc}\right)_{AB}} = \frac{\Delta n}{\alpha\left(\frac{dn}{dc}\right)_A + (1-\alpha)\left(\frac{dn}{dc}\right)_B}, \quad (3)$$

Where Δn is the variation of refractive index. Mass extinction coefficient of AB complex can be expressed as:

$$\varepsilon_{AB} = \alpha\varepsilon_A + (1-\alpha)\varepsilon_B \qquad (4)$$

By using Beer-Lambert equation and equation (4), C_{AB} can be expressed as follows:

$$C_{AB} = \frac{\mathrm{OD280nm}}{\alpha\varepsilon_A+(1-\alpha)\varepsilon_B}, \qquad (5)$$

By using equations (3) and (5), we obtain:

$$\frac{\Delta n}{\alpha\left(\frac{dn}{dc}\right)_A+(1-\alpha)\left(\frac{dn}{dc}\right)_B} = \frac{\mathrm{OD280nm}}{\alpha\varepsilon_A+(1-\alpha)\varepsilon_B} \qquad (6)$$

For which α can be inferred:

$$\alpha = \frac{\mathrm{OD280nm}\left(\frac{dn}{dc}\right)_B-\Delta n\,\varepsilon_B}{\Delta n\,(\varepsilon_A-\varepsilon_B)+OD280nm\left(\left(\frac{dn}{dc}\right)_A-\left(\frac{dn}{dc}\right)_B\right)} \qquad (7)$$

As dn/dc are identical, the term $OD280nm\left(\left(\frac{dn}{dc}\right)_A-\left(\frac{dn}{dc}\right)_B\right)$ is negligible. Therefore, the terms α, 1- α, C_A and C_B can be calculated by the protein-conjugate method and can be used in order to determine the molecular weights of protein A and protein B in a AB complex if ε_A and ε_B are significatively different. Concerning UbiK and UbiJ complex, the UbiJ extinction coefficient (0.951 ml/(mg.cm)) was predicted from the protein amino acid sequences with ProtParam tool (http://web.expasy.org/protparam/) and UbiK extinction coefficient was determined experimentally (0.059 ml/(mg.cm)) by using « UV extension from RI peak » method included into ASTRA software.

AUC-Sedimentation velocity experiments were conducted with a Beckman XL-I (Beckman-coulter, Palo Alto, USA) analytical ultracentrifuge (AUC) using an An-50Ti rotor. Increasing concentrations of UbiK and UbiK-UbiJ complexes P1 and P2 were loaded into Epon charcoal-filled two-sector 12 mm path-length cells. 400 µl of samples and 410 µl of buffer (50 mM Tris HCl pH 7.5, 150 mM NaCl) were centrifuged at 42,000 rpm (128 297g) and 20°C. Absorbance at 280 nm and interference scans were collected every 5 min and sedimentation velocity data were analyzed using SEDFIT software (38). Viscosity and density parameters were measured by using respectively Anton Paar microviscosimeter and density meter (DMA 4500). Partial specific volumes of proteins were predicted by SEDNTERP software.

Contrary to MSSV (Multi Signal Sedimentation Velocity) experiments (39) which require 3 signals (2 different wavelength in absorbance and interferometry) to determine protein stoichiometry, the present case is easier because the extinction coefficient of UbiK is close to zero (see SEC-MALS material and methods part). So the interferometric signal (ΔJ) is due to both complex components whereas absorbance signal is only due to UbiJ. $\Delta J_{UbiJ/UbiK}$, ΔJ_{UbiJ} and ΔJ_{UbiK} correspond to fringes displaced respectively due to UbiJ/UbiK complex, UbiJ and UbiK. $\varepsilon_{IF\ UbiJ}$, $\varepsilon_{IF\ UbiK}$ correspond to molar increments of UbiJ and UbiK in Rayleigh interferometry and ε_{UbiJ} corresponds to molar extinction coefficient at 280 nm (all three last parameters are predicted thanks to calculator module of SEDFIT software by using protein sequences). l is the path length of analytical ultracentrifugation centerpiece (1.2 cm).

$$\Delta J_{UbiJ/UbiK} = \Delta J_{UbiJ} + \Delta J_{UbiK} \quad (1)$$

Thanks to Equation 8 of Padrick (39), we can write:

$$\Delta J_{UbiJ} \cong \varepsilon_{IF\ UbiJ}\, l\, C_{UbiJ} \text{ and}$$
$$\Delta J_{UbiK} \cong \varepsilon_{IF\ UbiK}\, l\, C_{UbiK} \quad (2)$$

As only UbiJ absorbs we can apply the Beer-Lambert equation as followed:

$$OD280nm = \varepsilon_{UbiJ}\, l\, C_{UbiJ} \quad (3)$$

OD 280nm is the optical density at 280 nm. Finally, by combining equation (1), (2) and (3), we obtain:

$$\Delta J_{UbiJ/UbiK} - \varepsilon_{IF\ UbiJ}\, l\, \left(\frac{OD280nm}{l\, C_{UbiJ}}\right) = \Delta J_{UbiK} \quad (4)$$

$$\frac{\Delta J_{UbiJ/UbiK} - \varepsilon_{IF\ UbiJ}\left(\frac{OD280nm}{C_{UbiJ}}\right)}{\varepsilon_{IF\ UbiK}\ l} \cong C_{UbiK} \quad (5)$$

After integration of each peak obtained in c(s) distribution by SEDFIT, $\Delta J_{UbiJ/UbiK}$, OD280nm are determined, C_{UbiJ} and C_{UbiK} are calculated to obtain the molar ratio of UbiK and UbiJ in UbiK/UbiJ complex.

Fluorescence sedimentation velocity experiments were performed thanks to Aviv fluorescence detection system (AU-FDS) and UbiK was labelled by monolith NT-115 Blue NHS (Nanotemper Technology) according to the manufacturer's instructions. Labelled protein was diluted from 60 nM to 3 pM with the buffer cited previously; in order to prevent protein adsorption, BSA was added at final concentration of 0.1 mg/ml for the concentration of labelled UbiK bellow 1 nM. In order to study oligomeric state of UbiK at concentration higher than 60 nM, unlabelled UbiK was added to 60 nM of fluorescent protein in order to reach the desired concentration. Samples are sedimented in the same condition than Absorbance/Interference experiments except than no reference is required during fluorescence experiments.

Infection of macrophages with Salmonella enterica strains-RAW 264.7 macrophages were seeded at a density of 4.10^5 cells per well in 6-well tissue culture plates containing DMEM with 10% fetal bovine serum (FBS) (HyClone). *S. enterica* strains were grown over-night with or without oxygen and at 30°C or 37°C as indicated in the figure legend. Afterwards, these cultures were opsonized in DMEM containing FBS and normal mouse serum (10%, Perbio) for 30 minutes. Bacteria were added to the monolayers at a multiplicity of infection 10:1, centrifuged at 400 *g* for 5 min at 4°C, and incubated for 30 min at 37°C in 5% CO2. The macrophages were washed three times, and incubated with DMEM containing FBS and 100 µg/ml gentamicin for 60 minutes, after which the gentamicin concentration was decreased to 10 µg/ml for the remainder of the experiment. For enumeration of intracellular bacteria, macrophages were washed two times with PBS, lysed with 0.1% Triton X-100, and a dilution series was plated on LB agar.

Virulence assays in mice-Eight-week-old female BALB/c mice (Charles River Laboratories) were inoculated intraperitoneally with equal amounts of *S. enterica* wild-type and *ubiK* mutant strains for a total of 10^5 bacteria per mouse. The spleens were harvested 48 hours after inoculation, then homogenized. Bacteria were recovered and enumerated after plating a dilution series onto LB agar and LB agar with kanamycin. Competitive indexes (CI) were determined for each mouse. The CI is defined as the ratio between *ubiK* mutant and wild-type strains within the output (bacteria recovered from the mouse after infection) divided by their ratios within the input (initial inoculum).

Statistical methods-Results are presented as mean ± s.e.m. Data sets were compared by unpaired two-tailed *t*-test or an analysis of variance (ANOVA) using GraphPad Prism 7 software.

Aknowledgments
Thanks to the FB group for discussions and suggestions. This work was supported by the Agence Nationale de la Recherche (ANR), ANR Blanc (An)aéroUbi ANR-15-CE11-0001-02, Aix-Marseille Université (AMU), The Centre National de la Recherche Scientifique (CNRS - PICS07279) and the French State Program 'Investissements d'Avenir' (Grants "LABEX DYNAMO", ANR-11-LABX-0011). This work has benefited from the facilities and expertise of the Macromolecular Interaction Platform of I2BC (UMR 9198) supported by FRISBI.

Conflict of interest
The authors declare that they have no conflicts of interest with the contents of this article.

Author contributions: FB, FP, MF, ML and LA conceived and designed the experiments. LL, CF, LA, MHC, SBH, BF, DH, CMD, BR, LP and CV performed the experiments. DC ran mass spectrometry analyses. JC contributed reagents/materials/analysis tools. FB, FP, MF, ML and LA wrote the paper. All authors analysed the results and approved the final version of the manuscript.

REFERENCES

1. Nowicka, B., and Kruk, J. (2010) Occurrence, biosynthesis and function of isoprenoid quinones. *Biochim. Biophys. Acta*. **1797**, 1587–1605
2. Collins, M. D., and Jones, D. (1981) Distribution of isoprenoid quinone structural types in bacteria and their taxonomic implication. *Microbiol. Rev.* **45**, 316–354
3. Zhi, X.-Y., Yao, J.-C., Tang, S.-K., Huang, Y., Li, H.-W., and Li, W.-J. (2014) The futalosine pathway played an important role in menaquinone biosynthesis during early prokaryote evolution. *Genome Biol. Evol.* **6**, 149–160
4. Schoepp-Cothenet, B., Lieutaud, C., Baymann, F., Verméglio, A., Friedrich, T., Kramer, D. M., and Nitschke, W. (2009) Menaquinone as pool quinone in a purple bacterium. *Proc. Natl. Acad. Sci. U. S. A.* **106**, 8549–8554
5. Ravcheev, D. A., and Thiele, I. (2016) Genomic Analysis of the Human Gut Microbiome Suggests Novel Enzymes Involved in Quinone Biosynthesis. *Front. Microbiol.* **7**, 128
6. Aussel, L., Pierrel, F., Loiseau, L., Lombard, M., Fontecave, M., and Barras, F. (2014) Biosynthesis and physiology of coenzyme Q in bacteria. *Biochim. Biophys. Acta*. **1837**, 1004–1011
7. Hajj Chehade, M., Loiseau, L., Lombard, M., Pecqueur, L., Ismail, A., Smadja, M., Golinelli-Pimpaneau, B., Mellot-Draznieks, C., Hamelin, O., Aussel, L., Kieffer-Jaquinod, S., Labessan, N., Barras, F., Fontecave, M., and Pierrel, F. (2013) ubiI, a new gene in Escherichia coli coenzyme Q biosynthesis, is involved in aerobic C5-hydroxylation. *J. Biol. Chem.* **288**, 20085–20092
8. Alexander, K., and Young, I. G. (1978) Alternative hydroxylases for the aerobic and anaerobic biosynthesis of ubiquinone in Escherichia coli. *Biochemistry (Mosc.)*. **17**, 4750–4755
9. Aussel, L., Loiseau, L., Hajj Chehade, M., Pocachard, B., Fontecave, M., Pierrel, F., and Barras, F. (2014) ubiJ, a new gene required for aerobic growth and proliferation in macrophage, is involved in coenzyme Q biosynthesis in Escherichia coli and Salmonella enterica serovar Typhimurium. *J. Bacteriol.* **196**, 70–79
10. Wang, K.-C., Huang, C.-H., Ding, S.-M., Chen, C.-K., Fang, H.-W., Huang, M.-T., and Fang, S.-B. (2016) Role of yqiC in the Pathogenicity of Salmonella and Innate Immune Responses of Human Intestinal Epithelium. *Front. Microbiol.* **7**, 1614
11. Nichols, R. J., Sen, S., Choo, Y. J., Beltrao, P., Zietek, M., Chaba, R., Lee, S., Kazmierczak, K. M., Lee, K. J., Wong, A., Shales, M., Lovett, S., Winkler, M. E., Krogan, N. J., Typas, A., and Gross, C. A. (2011) Phenotypic landscape of a bacterial cell. *Cell*. **144**, 143–156
12. Poon, W. W., Davis, D. E., Ha, H. T., Jonassen, T., Rather, P. N., and Clarke, C. F. (2000) Identification of Escherichia coli ubiB, a gene required for the first monooxygenase step in ubiquinone biosynthesis. *J. Bacteriol.* **182**, 5139–5146
13. Hsu, A. Y., Poon, W. W., Shepherd, J. A., Myles, D. C., and Clarke, C. F. (1996) Complementation of coq3 mutant yeast by mitochondrial targeting of the Escherichia coli UbiG polypeptide: evidence that UbiG catalyzes both O-methylation steps in ubiquinone biosynthesis. *Biochemistry (Mosc.)*. **35**, 9797–9806
14. Federowicz, S., Kim, D., Ebrahim, A., Lerman, J., Nagarajan, H., Cho, B., Zengler, K., and Palsson, B. (2014) Determining the control circuitry of redox metabolism at the genome-scale. *PLoS Genet.* **10**, e1004264
15. Mason, J. M., and Arndt, K. M. (2004) Coiled coil domains: stability, specificity, and biological implications. *Chembiochem Eur. J. Chem. Biol.* **5**, 170–176
16. Chen, Z., Borek, D., Padrick, S. B., Gomez, T. S., Metlagel, Z., Ismail, A. M., Umetani, J., Billadeau, D. D., Otwinowski, Z., and Rosen, M. K. (2010) Structure and control of the actin regulatory WAVE complex. *Nature*. **468**, 533–538
17. Derivery, E., Fink, J., Martin, D., Houdusse, A., Piel, M., Stradal, T. E., Louvard, D., and Gautreau, A. (2008) Free Brick1 is a trimeric precursor in the assembly of a functional wave complex. *PloS One*. **3**, e2462
18. Karimova, G., Pidoux, J., Ullmann, A., and Ladant, D. (1998) A bacterial two-hybrid system based on a reconstituted signal transduction pathway. *Proc. Natl. Acad. Sci. U. S. A.* **95**, 5752–5756

19. Stolowich, N. J., Petrescu, A. D., Huang, H., Martin, G. G., Scott, A. I., and Schroeder, F. (2002) Sterol carrier protein-2: structure reveals function. *Cell. Mol. Life Sci. CMLS.* **59**, 193–212
20. De Berti, F. P., Capaldi, S., Ferreyra, R., Burgardt, N., Acierno, J. P., Klinke, S., Monaco, H. L., and Ermácora, M. R. (2013) The crystal structure of sterol carrier protein 2 from Yarrowia lipolytica and the evolutionary conservation of a large, non-specific lipid-binding cavity. *J. Struct. Funct. Genomics*. **14**, 145–153
21. Dyer, D. H., Lovell, S., Thoden, J. B., Holden, H. M., Rayment, I., and Lan, Q. (2003) The structural determination of an insect sterol carrier protein-2 with a ligand-bound C16 fatty acid at 1.35-A resolution. *J. Biol. Chem.* **278**, 39085–39091
22. García, F. L., Szyperski, T., Dyer, J. H., Choinowski, T., Seedorf, U., Hauser, H., and Wüthrich, K. (2000) NMR structure of the sterol carrier protein-2: implications for the biological role. *J. Mol. Biol.* **295**, 595–603
23. Haapalainen, A. M., van Aalten, D. M., Meriläinen, G., Jalonen, J. E., Pirilä, P., Wierenga, R. K., Hiltunen, J. K., and Glumoff, T. (2001) Crystal structure of the liganded SCP-2-like domain of human peroxisomal multifunctional enzyme type 2 at 1.75 A resolution. *J. Mol. Biol.* **313**, 1127–1138
24. Carrica, M. C., Craig, P. O., García-Angulo, V. A., Aguirre, A., García-Véscovi, E., Goldbaum, F. A., and Cravero, S. L. (2011) YqiC of Salmonella enterica serovar Typhimurium is a membrane fusogenic protein required for mice colonization. *BMC Microbiol.* **11**, 95
25. Beuzón, C. R., and Holden, D. W. (2001) Use of mixed infections with Salmonella strains to study virulence genes and their interactions in vivo. *Microbes Infect. Inst. Pasteur*. **3**, 1345–1352
26. González-Mariscal, I., García-Testón, E., Padilla, S., Martín-Montalvo, A., Pomares-Viciana, T., Vazquez-Fonseca, L., Gandolfo-Domínguez, P., and Santos-Ocaña, C. (2014) Regulation of coenzyme Q biosynthesis in yeast: a new complex in the block. *IUBMB Life*. **66**, 63–70
27. Marbois, B., Gin, P., Gulmezian, M., and Clarke, C. F. (2009) The yeast Coq4 polypeptide organizes a mitochondrial protein complex essential for coenzyme Q biosynthesis. *Biochim. Biophys. Acta*. **1791**, 69–75
28. Floyd, B. J., Wilkerson, E. M., Veling, M. T., Minogue, C. E., Xia, C., Beebe, E. T., Wrobel, R. L., Cho, H., Kremer, L. S., Alston, C. L., Gromek, K. A., Dolan, B. K., Ulbrich, A., Stefely, J. A., Bohl, S. L., Werner, K. M., Jochem, A., Westphall, M. S., Rensvold, J. W., Taylor, R. W., Prokisch, H., Kim, J.-J. P., Coon, J. J., and Pagliarini, D. J. (2016) Mitochondrial Protein Interaction Mapping Identifies Regulators of Respiratory Chain Function. *Mol. Cell*. **63**, 621–632
29. Marteyn, B., Scorza, F. B., Sansonetti, P. J., and Tang, C. (2011) Breathing life into pathogens: the influence of oxygen on bacterial virulence and host responses in the gastrointestinal tract. *Cell. Microbiol.* **13**, 171–176
30. Datsenko, K. A., and Wanner, B. L. (2000) One-step inactivation of chromosomal genes in Escherichia coli K-12 using PCR products. *Proc. Natl. Acad. Sci. U. S. A.* **97**, 6640–6645
31. Pelosi, L., Ducluzeau, A.-L., Loiseau, L., Barras, F., Schneider, D., Junier, I., and Pierrel, F. (2016) Evolution of Ubiquinone Biosynthesis: Multiple Proteobacterial Enzymes with Various Regioselectivities To Catalyze Three Contiguous Aromatic Hydroxylation Reactions. *mSystems*. 10.1128/mSystems.00091-16
32. Bouveret, E., and Brun, C. (2012) Bacterial interactomes: from interactions to networks. *Methods Mol. Biol. Clifton NJ*. **804**, 15–33
33. Golemis, E. A., Giurys, J., and Brent, R. (1994) Two hybrid systems/interaction traps. in *The bacteriophages*, John Wiley & Sons, Calendar, R., New York
34. Whitmore, L., and Wallace, B. A. (2008) Protein secondary structure analyses from circular dichroism spectroscopy: methods and reference databases. *Biopolymers*. **89**, 392–400
35. Louis-Jeune, C., Andrade-Navarro, M. A., and Perez-Iratxeta, C. (2012) Prediction of protein secondary structure from circular dichroism using theoretically derived spectra. *Proteins*. **80**, 374–381
36. Veesler, D., Blangy, S., Siponen, M., Vincentelli, R., Cambillau, C., and Sciara, G. (2009) Production and biophysical characterization of the CorA transporter from Methanosarcina mazei. *Anal. Biochem.* **388**, 115–121

37. Zhao, H., Brown, P. H., and Schuck, P. (2011) On the distribution of protein refractive index increments. *Biophys. J.* **100**, 2309–2317
38. Schuck, P. (2000) Size-distribution analysis of macromolecules by sedimentation velocity ultracentrifugation and lamm equation modeling. *Biophys. J.* **78**, 1606–1619
39. Padrick, S. B., Deka, R. K., Chuang, J. L., Wynn, R. M., Chuang, D. T., Norgard, M. V., Rosen, M. K., and Brautigam, C. A. (2010) Determination of protein complex stoichiometry through multisignal sedimentation velocity experiments. *Anal. Biochem.* **407**, 89–103

The abbreviations used are: UQ, ubiquinone; MK, menaquinone; DMK, demethylmenaquinone; OPP, 3-octaprenylphenol; SEC-MALS, multi-angle light scattering coupled to size exclusion chromatography; SCP, sterol carrier protein; AUC, analytical ultracentrifuge (AUC).

FIGURE LEGENDS

FIGURE 1. A) HPLC-electrochemical detection (ECD) analyses of lipid extracts from 1 mg of *E. coli* WT or Δ*ubiK* cells transformed with either the empty pK vector (vec) or the pK vector carrying the *ubiK* gene grown in LB medium in aerobic conditions. The chromatograms are representative of three independent experiments. The peaks corresponding to ubiquinone (UQ_8), demethylmenaquinone (DMK_8), 3-octaprenylphenol (OPP) and the coenzyme Q_{10} (UQ_{10}) standard are indicated. **B**) Quantification of cellular UQ_8 content of the *E. coli* strains described in A) based on ECD signal (peak area). **C and D**) Quantification (peak area) of cellular DMK_8 and MK_8 from chromatograms at 247 nm (see Fig. S1B). **E**) Quantification (peak area) of OPP from chromatograms at 275 nm (see Fig. S1D). **B-E**, Mean ± s.e.m.; n=3-5; n, number of independent experiments; ***: $P<0.001$, ****: $P<0.0001$, One-way ANOVA. **F**) ECD quantification of cellular UQ_8 content of the *E. coli* WT and Δ*ubiK* cells grown in anaerobic conditions in LB medium; n=3. **G**) Immunodetection of SPA-tagged proteins UbiE, UbiK and UbiJ after growth in LB medium under aerobic ($+O_2$) or anaerobic ($-O_2$) conditions. Equal loading was verified with immunodetection of the protein LamB and staining of the SDS-PAGE with Coomassie blue dye. Mw: molecular weights.

FIGURE 2. A) SEC-MALS analysis of UbiK from *E. coli* (injection of 100 µl of UbiK at 2 mg/ml on a Superdex 200 10/300 GL increase column, 50 mM Tris-HCl, 150 mM NaCl buffer, pH 7.5. Solid and blue lines correspond to refraction index signal and molar mass respectively. **B**) Far-UV circular dichroism spectrum (185-260 nm) of *E. coli* UbiK (50 mM Tris-HCl, 150 mM NaCl buffer, pH 7.5).

FIGURE 3. **A**) Crystal structure of the alpha-helical coiled-coil Brick1 homotrimer from *Dictyostelium discoideum* (PDB code 3PP5); **B**) Predicted structural model of *E.coli* UbiK (Swiss Model); **C**) Hypothesized model of the alpha-helical coiled-coil UbiK homotrimer, based on sequence identity, CD and SEC-MALLS. N and C-termini are predicted as disordered regions

FIGURE 4. Interactions between UbiK and the other Ubi proteins. A bacterial two-hybrid system was used to detect in vivo protein-protein interactions. Values of β-galactosidase activities, calculated in Miller Units, with standard errors are shown: pT25-*ubiK* (**A**) or pT18-*ubiK* (**B**) were analyzed with *ubiJ*, *E*, *I*, *K*, *B*, *D*, *G*, *A*, *X*, *H* or *F* genes respectively.

FIGURE 5. A) UbiJ-His and UbiK-Stag were co-expressed from the pETDuet-6his-*ubiJ*/*ubiK*-Stag plasmid. Cell extracts were passed over a Ni-NTA column. Imidazole gradient was applied and the two proteins were co-eluted. Lane 1: soluble cell extract; Lane 2: flow through; Lane 3: wash; Lanes 4-9: imidazole eluted peak fractions. **B)** Pool-down assays were carried out to investigate the interactions between the UbiK and UbiJ proteins. *UbiK*, *ubiJ* and *sufC* (negative control) genes were fused at their 5′-end with the *malE* gene and the chimeric proteins were purified in *His_6-ubiJ* (lanes 1 and 2) or *ubiK-SPA* (lanes 3 and 4) backgrounds. Soluble extracts of each strain were loaded onto an amylose column, the column was washed and a solution of maltose was applied. MBP-UbiK and His_6-UbiJ were co-eluted (lane 2) as MBP–UbiJ and UbiK-SPA (lane 4). **C**) Interactions between UbiK and UbiJ (top), UbiK and the 50 C-terminal amino acids of UbiJ (middle), and UbiK and an empty plasmid (bottom) were

analyzed by a yeast two-hybrid reporter system. Diploid strains producing pairs of Ubi proteins were tested on solid medium for activation of the *lacZ* gene and the intensity of interaction was monitored by a gradient from dark blue (strong interaction) to white (no interaction) (left). The ability to growth on selective medium lacking leucine was also monitored during 16 hours at 30°C (right).

FIGURE 6. SEC-MALS analysis of the two complexes P1 (**A**) and P2 (**B**) of UbiK-UbiJ. Samples were run on a Superdex 200 Increase 10/300 GL. Blue, red and green curves correspond to the molar masses of UbiK-UbiJ complex, UbiK and UbiJ respectively (protein-conjugate method). C) Crystal structure of the Sterol carrier protein SCP2 from *Yarrowia lipolytica*, with palmitic acid ligand. D) Hypothesized model of the E.coli UbiK-UbiJ 2:1 heterotrimer complex, made by Phyre 2. UbiJ monomer is coloured orange, UbiK dimer is coloured blue and red. The template for the N-terminal domain of UbiJ (1-120) was 4JGX (SCP2 from *Yarrowia lipolytica*); the template for the C-terminal domain (151-195) was 3QH9 (human coiled-coil liprin) and the template for the middle domain (132-150) was 1M1J (fibrinogen alpha subunit)

FIGURE 7. ESI-TOF-MS of UbiK-UbiJ P2 supernatant. The m/z 263.22 seen in UbiK-UbiJ sample corresponds to the exact mass of palmitoleic acid, m/z 263.23 (commercial standard inset).

FIGURE 8. A) UQ_8 content of *S. enterica* WT and Δ*ubiK cells* after growth at 37°C in LB medium in aerobic (O_2) or anaerobic conditions. Mean ± s.e.m.; n=4, ns: Non significant, ****: $P<0.0001$, unpaired two-tailed t test. **B** and **C**) *Salmonella* strains (WT and Δ*ubiK*) were grown over-night under aerobic (grey bars, **B**) or anaerobic conditions (black bars, **B**) in LB at 37°C. Opsonized bacteria were phagocytosed by RAW 264.7 cells. The experiments were carried out at 37°C (grey bars, **C**) or 30°C (black bars, **C**). Two and 16 hours post-infection, mouse macrophages were lysed for enumeration of intracellular bacteria (gentamicin-protected) determined by colony-forming unit (cfu) counts. The values shown represent the proliferation index calculated as a ratio of the intracellular bacteria between 16 and 2 hours post-infection. Results are the means ± standard deviation of at least three independent experiments each in triplicate. Asterisks indicate a statistically significant difference between the *ubiK* mutant and the WT. *P ≤ 0.05 (Mann-Whitney U test). **D**) BALB/c mice were inoculated intraperitoneally with a 1:1 mixture of *ubiK* mutant and wild-type *Salmonella* strains. Forty-eight hours post-inoculation, spleens were harvested for bacterial counts. Competitive indexes of wild-type versus *ubiK* mutant strains in mice were determined. Each circle represents one mouse and the horizontal bar corresponds to the mean. A one-sample t test was used to determine whether the CI was significantly different from 1. ***P ≤ 0.001.

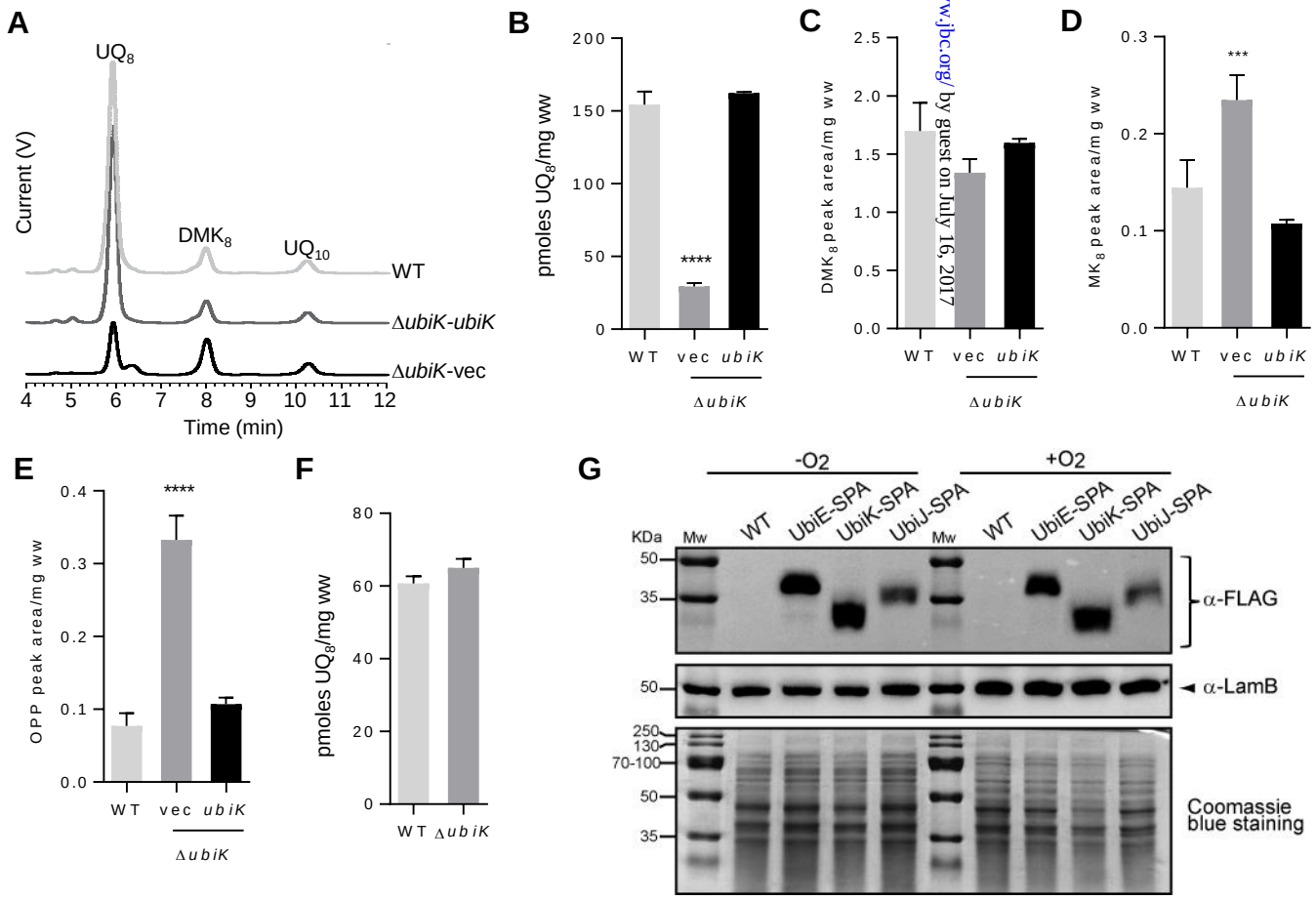

Figure 1

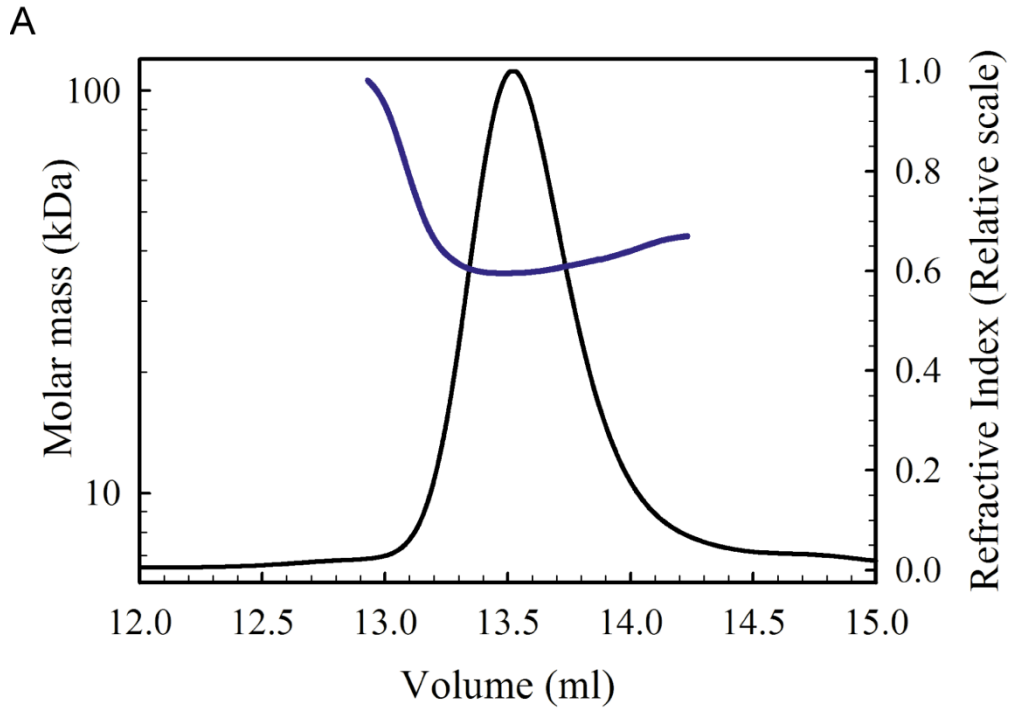

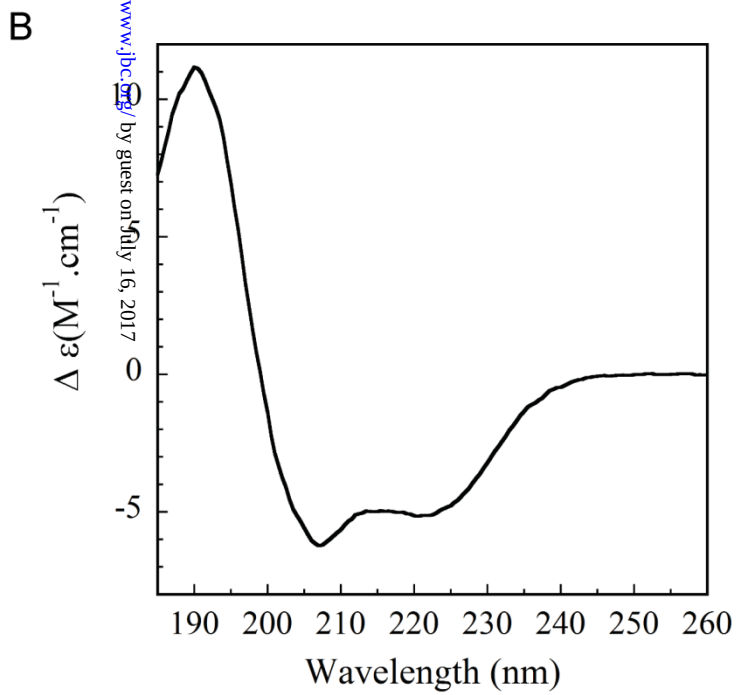

Figure 2

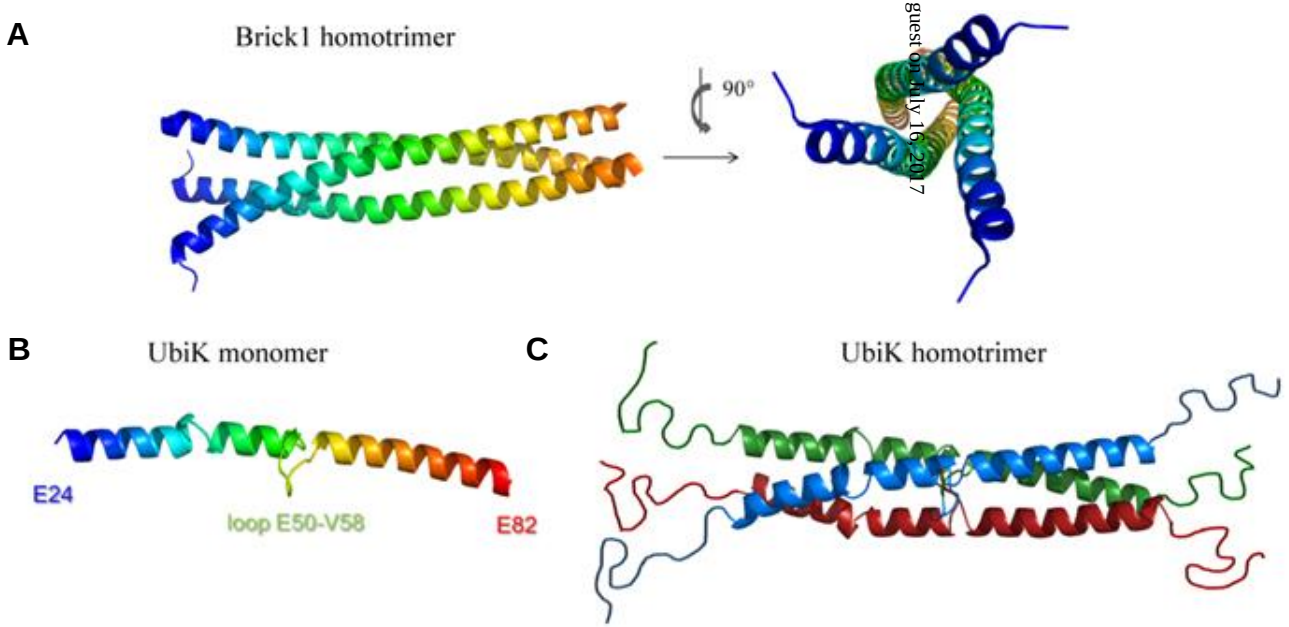

Figure 3

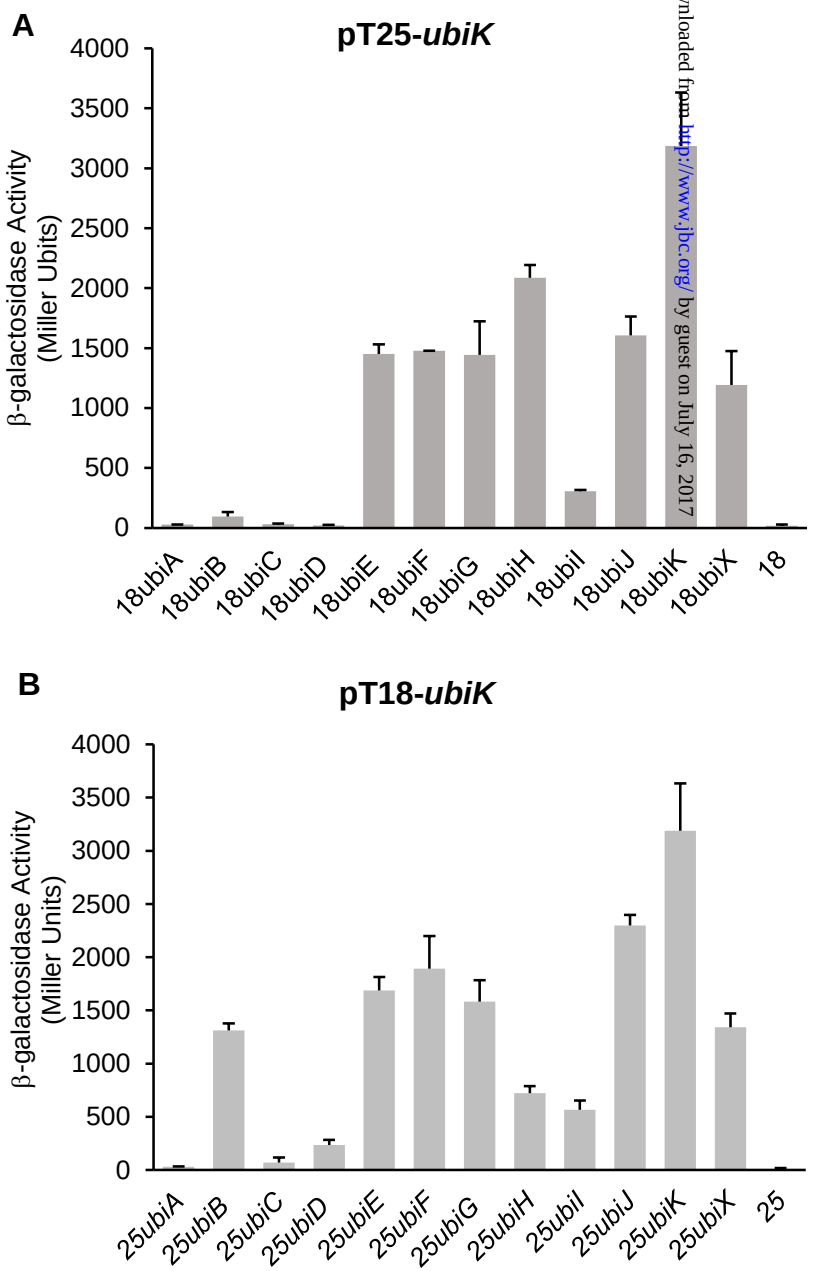

Figure 4

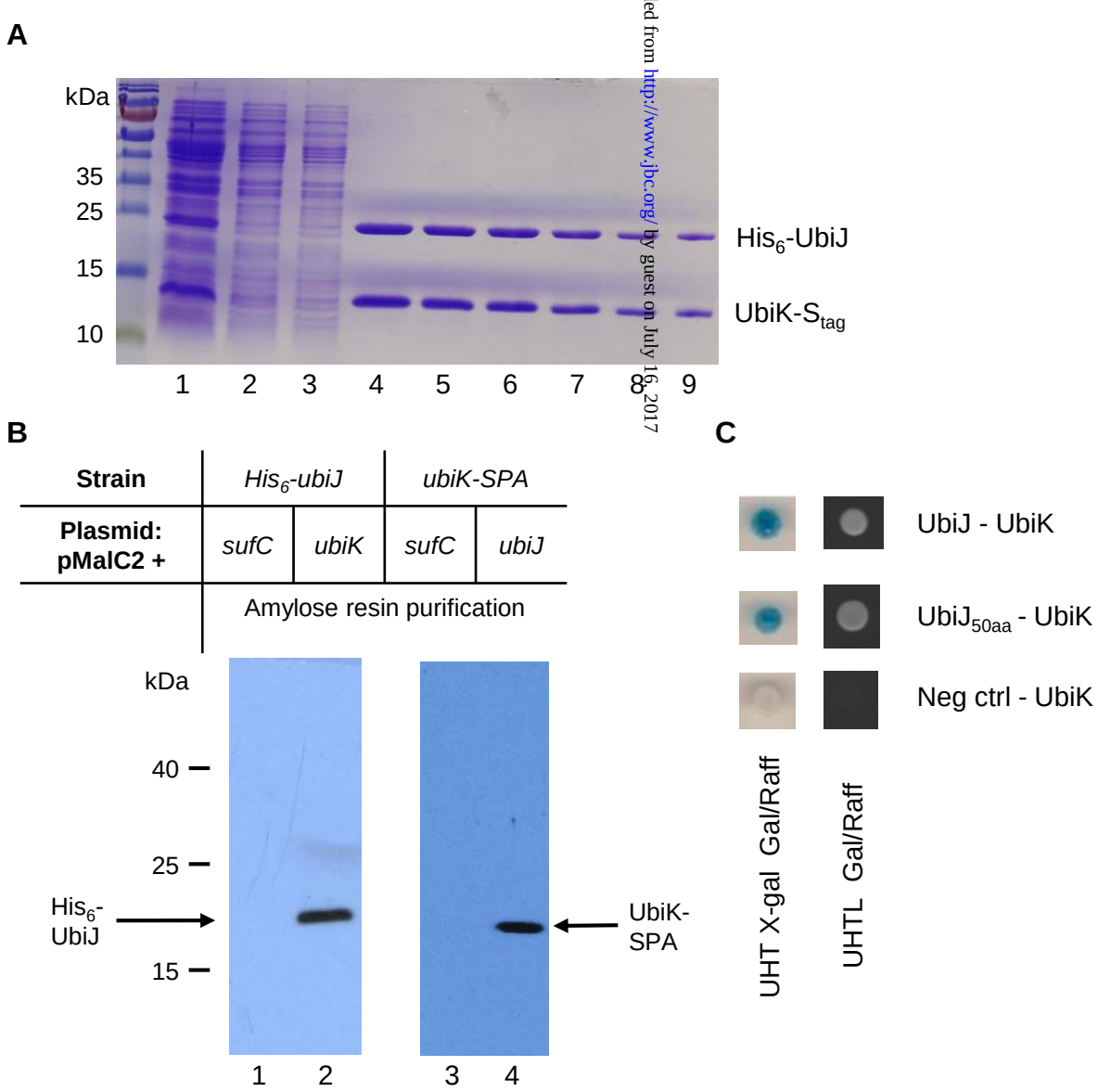

Figure 5

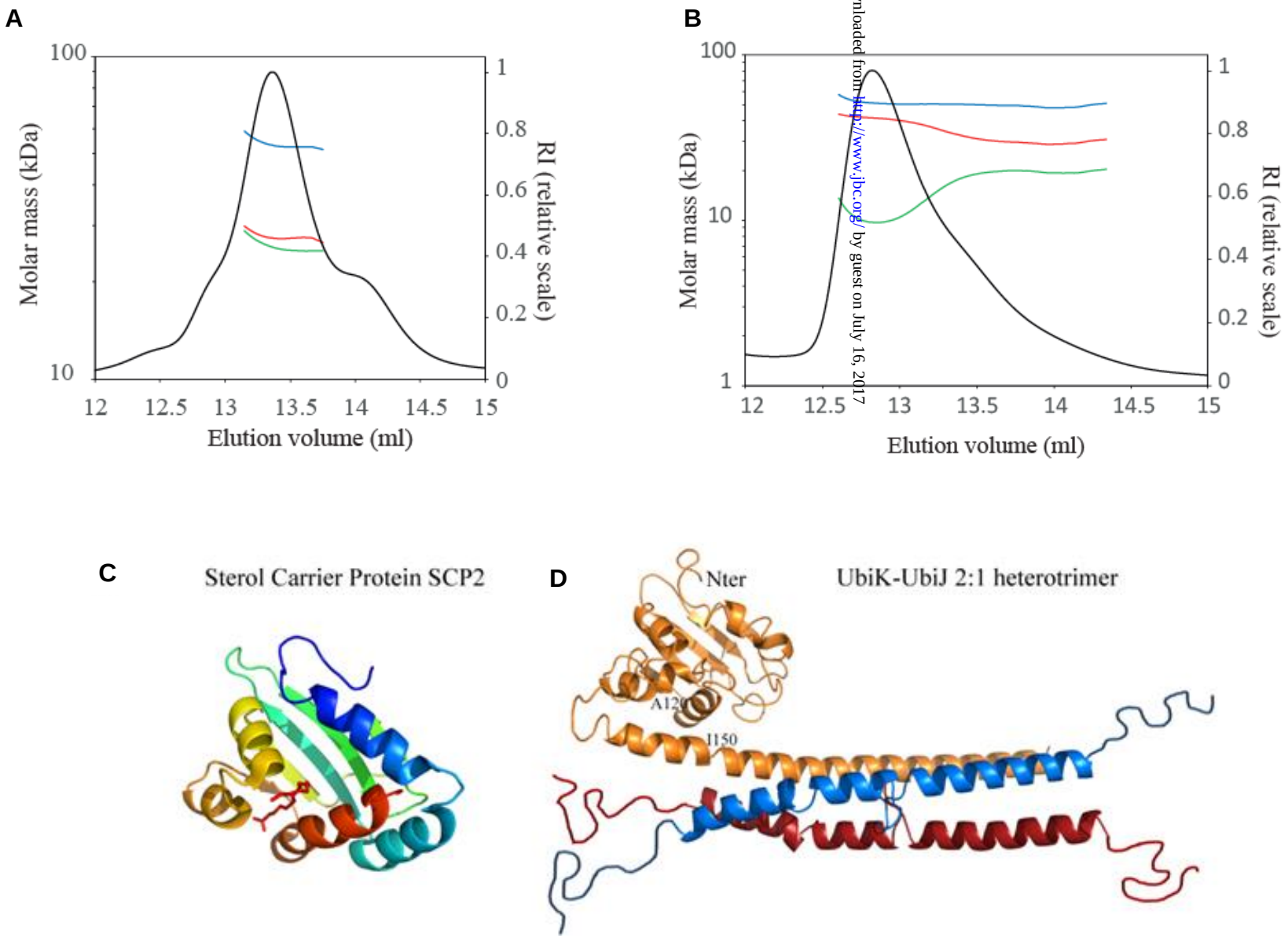

Figure 6

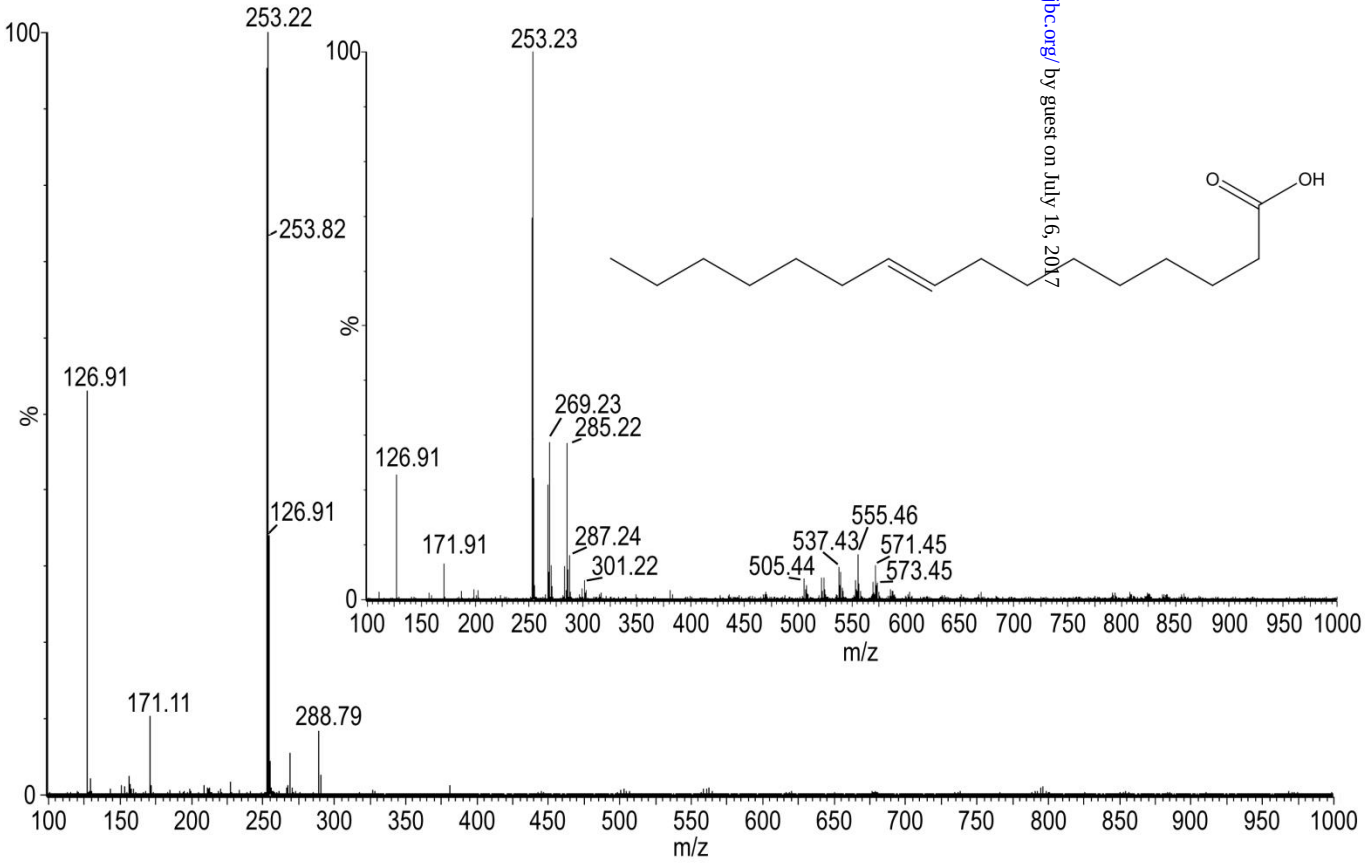

Figure 7

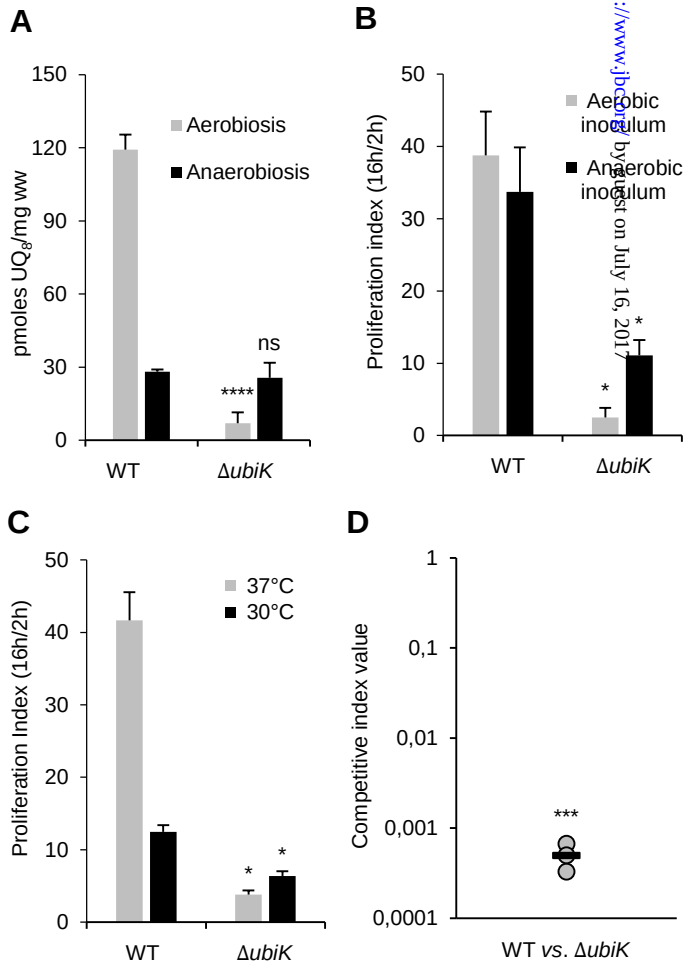

Figure 8

The UbiK protein is an accessory factor necessary for bacterial ubiquinone (UQ) biosynthesis and forms a complex with the UQ biogenesis factor UbiJ

Laurent Loiseau, Cameron Fyfe, Laurent Aussel, Mahmoud Hajj Chehade, Sara B. Hernández, Bruno Faivre, Djemel Hamdane, Caroline Mellot-Draznieks, Bérengère Rascalou, Ludovic Pelosi, Christophe Velours, David Cornu, Murielle Lombard, Josep Casadesús, Fabien Pierrel, Marc Fontecave and Frédéric Barras

J. Biol. Chem. published online May 30, 2017
